The use of PDF analysis to investigate local structure and domains

G. Paglia*, E. S. Bozin* and S. J. L. Billinge*

*Michigan State University, East Lansing, MI, USA, paglia@msu.edu, bozin@pa.msu.edu, billinge@pa.msu.edu

ABSTRACT

Knowledge of the atomic-scale structure is an important prerequisite to understand and control the properties of materials. This is becoming increasingly important with the growing use of nanostructured materials with limited structural coherence but it is becoming increasingly difficult to confidently elucidate information using traditional characterization techniques. One technique which compliments existing methods is the atomic pair distribution function (PDF) method. This is a total scattering approach whereby both the diffuse and Bragg scattering components of diffraction patterns are considered, enabling a quantitative assessment of the local structures of disordered materials. By studying the PDF on different length-scales we can obtain information concerning individual domains within nanostructured materials. Examples of how this technique can be applied are provided here.

Keywords: PDF, Bragg-scattering, diffuse-scattering, total-scattering.

1 INTRODUCTION

Two of the main techniques used to determine atomic structure are powder x-ray and neutron diffraction from which the Bragg peaks are used to determine the structure. These techniques can be difficult to apply to nanostructures, which have limited structural coherence resulting in large diffuse components in their diffraction patterns. However, the structure of nanomaterials can be elucidated through use of the atomic pair distribution function (PDF) [1,2]. This is simply another representation of the powder diffraction data; however, the data is represented in real-space and the diffuse scattering component is also directly measured. The PDF is formally defined by

$$G(r) = 4\pi r[\rho(r) - \rho_o], \quad (1)$$

where ρ_o is the average atomic number density, $\rho(r)$ is the atomic pair density and r is the radial distance [3]. It provides the probability of finding pairs of atoms separated by a distance r. The PDF is obtained by the sine Fourier transformation of the reciprocal space total scattering structure function $S(Q)$, obtained from a diffraction experiment. Because it derives from *both* Bragg and diffuse scattering components, it yields quantitative *total scattering* information about the local disorder within a material [2]. All diffracted intensities (Bragg and diffuse) are therefore equally considered, making it ideal for examining materials which have structural coherence at the nanometer length scales.

2 OBTAINING THE PDF

The PDF can be obtained using standard laboratory X-ray, synchrotron or neutron diffraction equipment. Typically, the main extra requirements for successful analysis are the collection of the environment background to subtract from the data, so that that the processed PDF contains signal stemming solely from the sample, and longer data collection times to achieve sufficient counting statistics in the high-Q (low-r) regions of the data. The data collection times using traditional experimental geometries are normally around 8 hours per data set, however, the recently developed RA-PDF procedure [4] allows a data set to be collected in as little as 3 minutes.

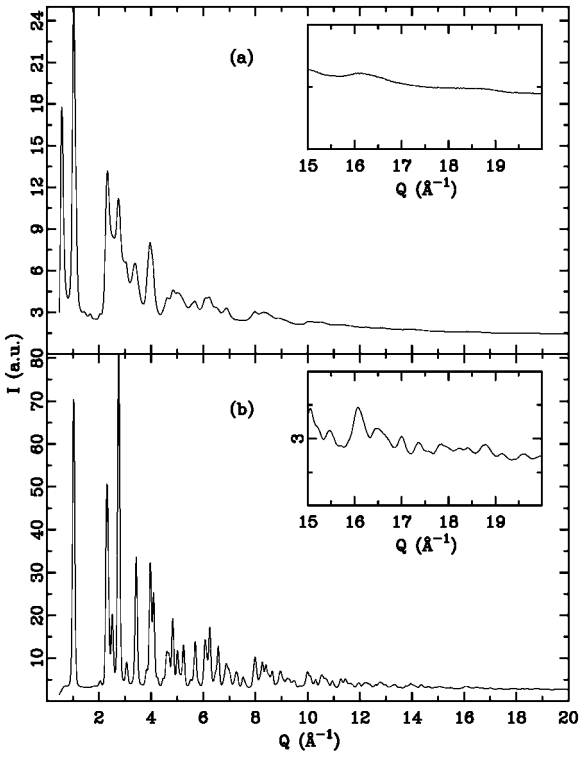

Figure 1. Experimental X-ray powder diffraction patterns for (a) nanocrystalline $LiMoS_2$ and (b) crystalline MoS_2 shown for comparison. The insets show amplified I(Q) data at high-Q.

The need for using the PDF method is highlighted in Figure 1, which displays the XRD pattern for nanocrystalline $LiMoS_2$ and crystalline MoS_2. The MoS_2 (Figure 1(b)) exhibits a relatively lower background and well-defined Bragg peaks up to a high wave vector $Q \sim 15 - 20$ Å^{-1} ($Q = 4\pi\sin\theta/\lambda$) due to the material being highly crystalline. By comparison, the $LiMoS_2$ sample contains fewer Bragg-like features and a considerably larger diffuse component. This is particularly evident when viewing the inset of Figure 1 (a) which shows the high-Q data on the same expanded scale as the inset in Figure 1(b); *i.e.* there are little or no visible Bragg diffraction peaks in the high-Q region of the $LiMoS_2$ data. Diffraction patterns such as that for the $LiMoS_2$ are characteristic of materials with nanoscale order.

The total scattering function *S(Q)*, extracted from the total diffracted intensity according to

$$S(Q) = \frac{I^{coh}(Q) - \sum c_i \left| f_i(Q) \right|^2}{\left| \sum c_i f_i(Q) \right|^2} + 1 \qquad (2)$$

where $I^{coh}(Q)$ is the measured scattering intensity and c_i and $f_i(Q)$ are the atomic concentration and x-ray scattering factor, respectively, for atomic species i [3], is derived for each sample. Both long-range atomic order represented by sharp Bragg peaks and local non-periodic structural imperfections manifested in the diffuse components of the diffraction pattern are reflected in the *S(Q)*. It is convenient to represent the data in real space to facilitate simpler interpretation of the structural information. A Fourier transformation of the reduced total scattering structure function, *F(Q) = Q[S(Q)-1]*, produces the real-space PDF:

$$G(r) = \frac{2}{\pi} \int_{Q_{mn}}^{Q_{\max}} Q[S(Q) - 1] \sin(Qr) dQ \qquad (3)$$

Here, Q is the magnitude of the wave vector, 2θ is the angle between the incoming and outgoing radiation, and λ is the wavelength of the x-ray radiation. The resulting PDFs for the data illustrated in Figure 1 are shown in Figure 2. The peaks in the PDF data below 2 Å are unphysical and can be neglected. They originate from unavoidable systematic errors in the data arising from noise at high-Q and termination effects due to the finite Q_{max} used. They are shown for the purpose of gauging the quality of the PDF and can be seen to die out to the level of the noise before the first physical peak, (Mo-S) at 2.43 Å. The data-reduction step to obtain the *F(Q)* results in an amplification of the important diffuse signal at high-Q, which provides critically important quantitative information about the local structure. This is translated into the *G(r)* which contains sharp well-defined peaks at low-r, indicative of a well-defined local structure (Figure 2(a)). This is somewhat neglected in the XRD pattern of $LiMoS_2$ (Figure 1(a)), which is dominated by strong Bragg peaks at low-Q, and illustrates how traditional XRD is predominantly sensitive to long-range order. In the case of the crystalline MoS_2 the sharp Bragg features throughout the XRD pattern translate to much sharper features throughout the *G(r)* (Figure 2(b)) giving it a spectrum that is characteristic of highly crystalline materials. Once the PDF is obtained the degree of structural coherence and the relationship between the local, intermediate and average structures can be directly assessed in real space. Moreover, an approach similar to Rietveld analysis can be followed to solve the local structure. The effectiveness of this method in solving the structures of disordered materials has been demonstrated previously [1,5,6].

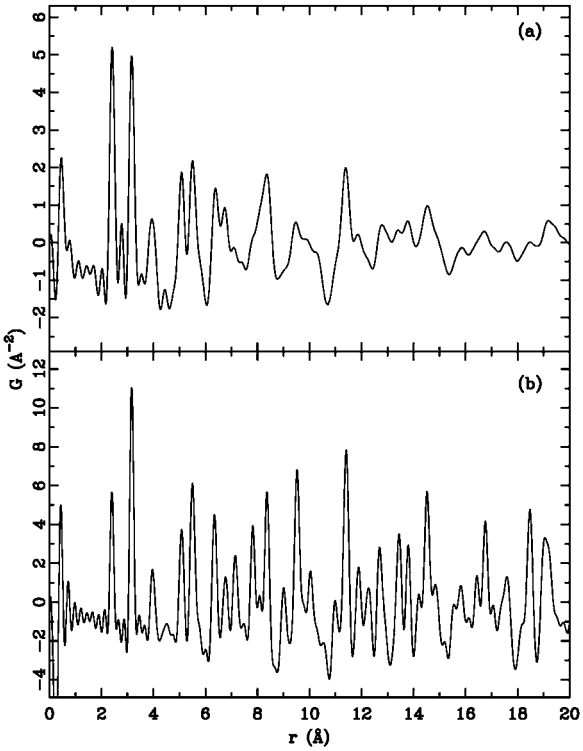

Figure 2. Experimental PDFs for (a) nanocrystalline $LiMoS_2$ and (b) crystalline MoS_2 shown for comparison. The insets show amplified I(Q) data at high-Q.

3 IDENTYFYING LOCAL DOMAINS

Not only can the PDF yield local structural information, it can also provide an indication of domain size. An illustrative example of this is provided in Figure 3. When nanodomains exist (as illustrated left in Figure 3) in the local structure and are not long-range ordered, the PDF at low-r (in the region less than approximately the dimension of the domains) will originate predominantly from pairs of atoms located within the domains (illustrated by the small arrows in Figure 3) and the local structure will be recovered from the data. At larger values of r, the PDF will originate from pairs where one atom is in one domain and the second is in another domain (illustrated by the larger arrows in Figure 3). In this regime the PDF will reflect the structure obtained by averaging over differently oriented and strained local domains. In this way, the PDF, depending on r,

provides both the intra and inter domain structure and crosses smoothly from the local structure to the average structure [7].

This is clearly illustrated if we consider solid fcc C_{60} as a nanostructured material where each bucky ball is a single domain (Figure 4). The bucky ball and its PDF, are shown in Figure 4. The diameter of the ball is 7.1 Å. Sharp peaks are observed in the PDF coming from the characteristic C-C pairs on the ball up to 7.1 Å. Thereafter, only broad featureless peaks exist in the PDF, indicative of the disordered fcc arrangement of the bucky balls. The sharp peaks are the intra-molecular structure and the broad features in the data are the inter-molecular structure, or ball-ball correlations. This separation of the intra- and inter-domain structure occurs as a natural consequence of the Fourier transform.

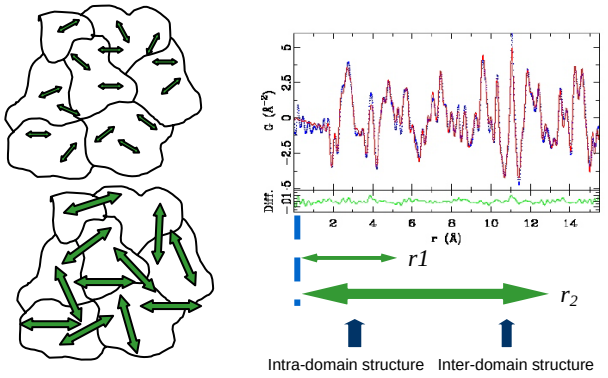

Figure 3. Illustrative example of the relationship between structural nanodomains and the origins of the PDF signal. See text for details.

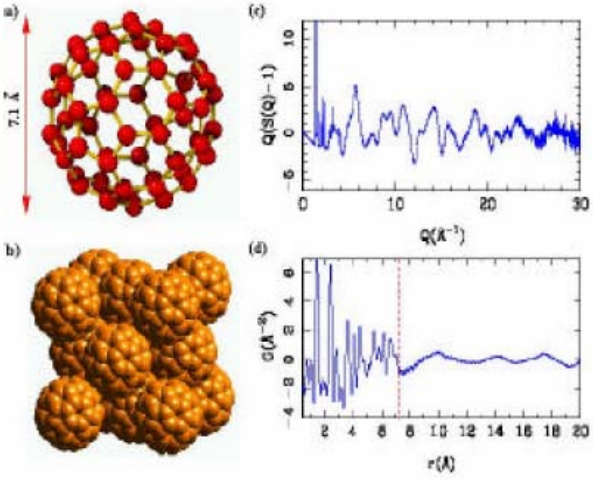

Figure 4. C_{60} (a and b), its normalized neutron diffraction pattern (c and d) and the corresponding PDF (d). The vertical dotted line in (d) is at 7.1 Å, the diameter of an individual bucky ball, as seen in (a). Figure taken from reference 8.

3.1 Sub-nm Length Scales in γ-Alumina

PDF analysis has recently been used to identify a previously undetected fine-scale nanostructure, over the range of 0-1 nm, in γ-alumina [9], which is an immensely important material industrially, particularly in catalysis (Figure 5). A description of the configuration was only possible by modifying the oxygen sublattice to reflect stacking faults with respect to the average structural model, which is itself controversial due to γ-alumina's 15-30 nm domain nanocrystalline nature [10,11,12]. The fine-scale structure was subsequently reconciled with the average structure, providing additional knowledge of the defect structure which should subsequently aid in better understanding of the surface structure and ultimately the functional properties.

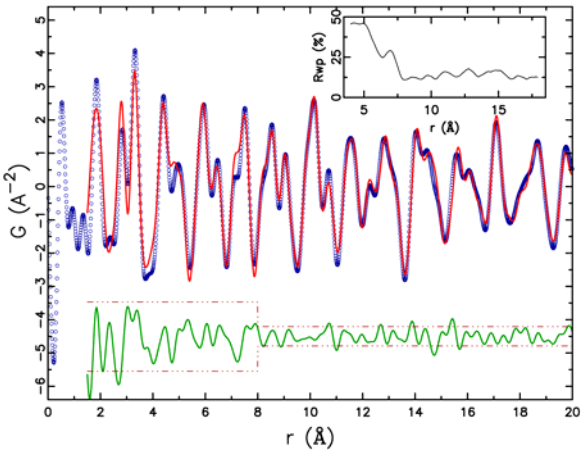

Figure 5. Comparison between the experimental PDF for γ-alumina (symbols) and the calculated PDF for the average model [10] fitted to the data (solid line). The solid line offset below each PDF shows the difference between the experimental and calculated PDF. The dashed line bordering the difference curves represents the 2σ standard deviation of all the points in the curves for the regions below and above r = 8 Å. An inset is shown illustrating the variation in R*wp* (the agreement factor) over the range of the PDF, emphasizing the sharp increase below 8 Å. The poor fit of the structural model below r = 8 Å indicates a different structural domain below 1 nm. Figure modified from reference 9.

Due to the short structural coherence of the 0-1 nm fine-scale nanostructure, it could not be solved crystallographically, necessitating a local structural approach. This demonstrates the power of total scattering methods in accurately resolving structural issues in nanostructured materials where traditional crystallographic methods fail.

4 CONCLUSIONS

We have demonstrated how the PDF method can be used to obtain quantitative, real-space information from disordered nanostructured materials with limited structural coherence, where standard powder diffraction techniques have difficulty. Its strength lies in with the ability to provide a quantitative measure of the diffuse scattering component of powder diffraction patterns in addition to the Bragg scattering that is considered in traditional crystallography. Further to providing an avenue for directly assessing the local structure configuration, it can also be used to investigate the relationship between structures on different length scales and assess the domain size. It is a powerful technique that can be utilized in isolation or in conjunction with a range of complementary techniques.

REFERENCES

[1] V. Petkov, P.Y. Zavalij, S. Lutta, M.S. Whittingham, V. Parvanov, and S. Shastri, Phys. Rev. B, 69, 085410, 2004.

[2] S.J.L. Billinge and M.G. Kanatzidis, Chem. Commun., 749-760, 2004.

[3] T. Egami and S.J.L. Billinge, "Underneath the Bragg Peaks - Structural Analysis of Complex Materials" (Pergamon, Amsterdam, 2003).

[4] P.J. Chupas, X. Qiu, J.C. Hanson, P.L. Lee, C.P. Grey, and S.J.L. Billinge, J. Appl. Crystallogr., 36, 1342, 2003.

[5] V. Petkov, S.J.L. Billinge, T. Vogt, A.S. Ichimura, and J.L. Dye, Phys. Rev. Lett., 89, 075502, 2002.

[6] G. Paglia, E.S. Bozin, D. Vengust, D. Mihailovic, and S.J.L. Billinge, Chem. Mater., 18, 100-106 2006.

[7] X. Qiu, T. Proffen, J.F. Mitchell, and S.J.L. Billinge, Phys. Rev. Lett., 94, 177203, 2005.

[8] S.J.L. Billinge, V. Petkov, and T. Proffen, IUCr Commission on Powder Diffraction Newsletter, 24, 21-22, 2000.

[9] G. Paglia, E. Bozin, and S.J.L. Billinge, Chem. Mater., submitted, 2006.

[10] G. Paglia, C.E. Buckley, A.L. Rohl, B.A. Hunter, R.D. Hart, J.V. Hanna and L.T. Byrne, Phys. Rev. B, 68, 144110, 2003.

[11] G. Paglia, C.E. Buckley, A.L. Rohl, R.D. Hart, K. Winter, A.J. Studer, B.A. Hunter, JV, Hanna, Chem. Mater., 16, 220-236, 2004.

[12] G. Paglia, C.E. Buckley, T.J. Udovic, A.L. Rohl, F. Jones, C.F. Maitland, and J. Connolly, Chem. Mater., 16, 1914-1923, 2004.